

# Tectonics

## RESEARCH ARTICLE

10.1029/2018TC004970

### Key Points:

- GPS geodetic data from the Bajo Segura GPS network (SE Spain) point to a NNW–SSE shortening and a N70E left-lateral component
- Our results indicate that part of the Eurasia–Nubia convergence is accommodated by the Eastern Betic Shear Zone
- Eurasia–Nubia plate convergence is transferred to the Eastern Betics because of an indenter of thin and rigid (possibly oceanic) crust

### Correspondence to:

I. Martín-Rojas,  
ivan.martin@ua.es

### Citation:

Borque, M. J., Sánchez-Alzola, A., Martín-Rojas, I., Alfaro, P., Molina, S., Rosa-Cintas, S., et al. (2019). How much Nubia–Eurasia convergence is accommodated by the NE end of the Eastern Betic Shear Zone (SE Spain)? Constraints from GPS velocities. *Tectonics*, 38, 1824–1839. <https://doi.org/10.1029/2018TC004970>

Received 12 JAN 2018






Accepted 14 APR 2019

Accepted article online 29 APR 2019

Published online 29 MAY 2019

©2019. American Geophysical Union.  
All Rights Reserved.

## How Much Nubia–Eurasia Convergence Is Accommodated by the NE End of the Eastern Betic Shear Zone (SE Spain)? Constraints From GPS Velocities

M. J. Borque<sup>1,2</sup>, A. Sánchez-Alzola<sup>3</sup> , I. Martín-Rojas<sup>4</sup> , P. Alfaro<sup>4</sup> , S. Molina<sup>4</sup> , S. Rosa-Cintas<sup>5</sup>, G. Rodríguez-Caderot<sup>6</sup>, C. de Lacy<sup>1,2</sup>, M. Avilés<sup>1</sup>, A. Herrera-Olmo<sup>1</sup>, F. J. García-Tortosa<sup>2,7</sup>, A. Estévez<sup>4</sup>, and A. J. Gil<sup>1,2</sup> 

<sup>1</sup>Departamento de Ingeniería Cartográfica, Geodésica y Fotogrametría, Universidad de Jaén, Jaén, Spain, <sup>2</sup>Centro de Estudios Avanzados en Ciencias de la Tierra CEACTierra, Universidad de Jaén, Jaén, Spain, <sup>3</sup>Departamento de Estadística e Investigación Operativa, Universidad de Cádiz, Puerto Real (Cádiz), Spain, <sup>4</sup>Departamento de Ciencias de la Tierra y del Medio Ambiente, Universidad de Alicante, Alicante, Spain, <sup>5</sup>Departamento de Didáctica General y Didácticas Específicas, Facultad de Educación, Universidad de Alicante, Alicante, Spain, <sup>6</sup>Departamento de Astronomía y Geodesia, Facultad de Matemáticas, Universidad Complutense de Madrid, Madrid, Spain, <sup>7</sup>Departamento de Geología, Universidad de Jaén, Jaén, Spain

**Abstract** We present the first GPS-derived geodetic observations from the NE end of the Eastern Betic Shear Zone obtained from the Bajo Segura GPS network (SE Spain). The network has 11 GPS sites and was sampled four times between 1999 and 2013. Despite the low signal-to-noise ratio of the residual velocities obtained, the velocities are nonzero at 95% confidence level. We postulate that the GPS data point to the partitioning of deformation into the NNW–SSE shortening and a N70E left-lateral component. The maximum deformation rates are located along the two main active faults in the study area. The maximum shortening rates (north component) in the southern region of the Bajo Segura Basin vary from west to east, ranging from 0.2 to 0.7 mm/year along the Bajo Segura Fault Zone. On the northern border of the basin, along the Crevillente Fault Zone, left-lateral displacement varies between 0.4 and 0.7 mm/year in the E–W direction. The GPS-based regional geodynamic models of the Western Mediterranean indicate that the residual shortening of the Eurasia–Nubia plate convergence is accommodated in the eastern part of the Iberian Peninsula and the Algero-Balearic Basin. Our results indicate that part of this residual deformation occurs at the NE end of the Eastern Betic Shear Zone, but significant deformation must be accommodated also to the north (External Betics) and to the south (Cartagena Basin and offshore area). We postulate that Eurasia–Nubia plate convergence is transferred to the Eastern Betics because of the thin and rigid (potentially oceanic) crust of the Algero-Balearic Basin, which acts as an indenter.

### 1. Introduction

The deformation of the diffuse plate boundary of Nubia and Eurasia in the Western Mediterranean is mainly concentrated in North Africa (North Algeria), although approximately one third of the total convergence is accommodated to the north, that is, in the Algero-Balearic Basin and the Eastern Betics (Koulali et al., 2011; Pérez-Peña et al., 2010; Serpelloni et al., 2007; Spakman et al., 2018; Vernant et al., 2010, among others). Within this general convergence regime, other tectonic processes are occurring in the westernmost part of the Western Mediterranean. These processes appear to be related to active subduction (e.g. Gutscher et al., 2002), deep-seated delamination processes (e.g. Fadil et al., 2006; Pérouse et al., 2010; Petit et al., 2015; May-Baratin et al., 2016, among others), or slab dragging (Spakman et al., 2018).

The Eastern Betic Shear Zone (EBSZ; Silva et al., 1993), part of the Trans-Alboran Shear Zone (De Larouzière et al., 1988) is one of the key active structures in the Western Mediterranean geodynamic regime (Figure 1a). The Bajo Segura Basin (Alicante province), which is located at the onshore NE end of the EBSZ, is one of the areas of the Iberian Peninsula that has exhibited the highest seismic hazard in recent centuries (IGN, 2018). Although this area is characterized by low-magnitude earthquakes,  $M > 5$  events occur occasionally (Buforn et al., 1995). The most destructive event was the 1829 Torrevieja earthquake (IMSK = IX–X;  $M_s = 6.3$ – $6.9$ ), which caused nearly 400 casualties (Muñoz & Udías, 1991). Another significant event occurred in 1919 in Jacarilla-Torremendo and was characterized by two events occurring 14 min apart ( $m_b = 5.1$  and  $5.2$ ).

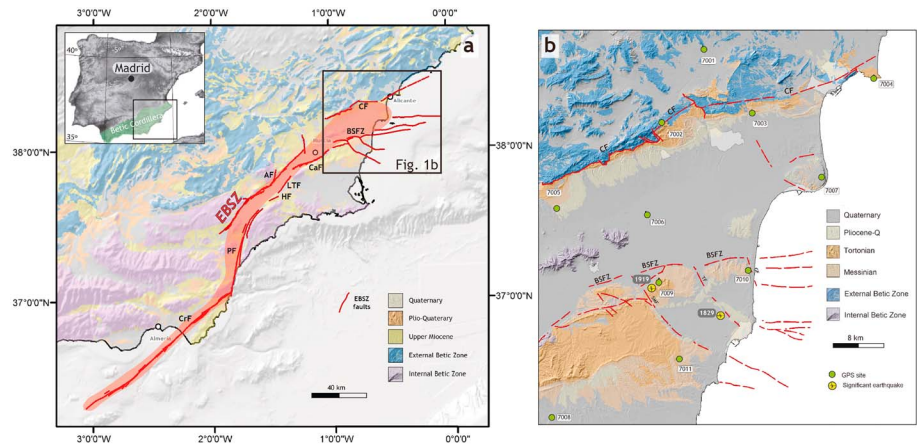


**Figure 1.** (a) Geological sketch map of the Eastern Betic Cordillera. Red lines represent the active faults of the Eastern Betic Shear Zone (EBSZ; CrF = Carboneras Fault, PF = Palomares Fault, AF = Alhama de Murcia Fault, HF = Hinojares Fault, LTF = Los Tollos Fault, CaF = Carrascoy Fault, BSFZ = Bajo Segura Fault Zone, CF = Crevillente Fault). The square indicates the location of Figure 1b. (b) Geological map of the Bajo Segura Basin. Significant earthquakes and locations of GPS stations of the Bajo Segura network are also shown.

Recently, several significant earthquakes occurred next to the study area, that is, in the western extent of the EBSZ and the Crevillente Fault (CF). A  $M = 5.2$  earthquake killed nine people and injured hundreds in Lorca in May 2011. Three earthquakes with a magnitude of approximately 5.0 occurred in Mula (1999), Bullas (2002), and Zarcilla de Ramos-La Paca (2005; Sanz de Galdeano & Buforn, 2005), between the EBSZ and the western sector of the CF. This seismic activity in the study area is related to slow-moving faults (approximately 1 mm/year or less) with seismic cycles of thousands of years (Alfaro et al., 2012; Taboada et al., 1993). In these geodynamic settings, it is necessary to integrate geologic (long-term) and geodetic (short-term) data to estimate fault slip rates to obtain more precise seismic hazard estimations.

Regional GPS networks have been used to estimate the geodynamics of the Eurasian-African plate boundary (see Nocquet, 2012, and references therein) or to improve the understanding of the geodynamics of some areas or specific active faults (De Guidi et al., 2013; Ferranti et al., 2014; Mueller et al., 2013, among others). Nevertheless, detailed studies on the basin scale are scarce in the Betic Cordillera. Several GPS networks in Zafarraya (Galindo Zaldívar et al., 2003), Granada (Gil et al., 2002; Ruiz et al., 2003), Balanegra-Almería (Marín-Lechado et al., 2010), and the Baza Fault (implemented in 2010) have been episodically measured to better understand the present-day deformation of the Central Betic Cordillera. In the Eastern Betic Cordillera, the CuaTeNeo GPS network (Echeverría et al., 2013) has provided very interesting results concerning the left-lateral deformation of the EBSZ. Nevertheless, there is a lack of geodetic information at the NE end of this key geodynamic structure in the Bajo Segura Basin; this information is limited to that provided by regional studies, as there is only one GPS site (ALAC, Alicante) in the entire study area.

We designed the GPS network of the Bajo Segura Basin, which contains 11 sites, in 1999 (Figure 1b). This network, which is located to the east of the CuaTeNeo GPS network (Echeverría et al., 2013, 2015), covers the seismogenic area of the 1829 Torrevieja earthquake and the 1919 Jacarilla-Torremendo earthquake. In this paper, we estimate, for the first time, the velocity field and strain rates of one of the areas with the highest seismic hazard in the Iberian Peninsula. We compute the GPS position time series using precise point positioning (PPP; Zumberge et al., 1997), and we obtain the velocity field using linear regression and the crustal strain rates in the region using the GRID\_STRAIN program (Teza et al., 2008). We also compare these results with those obtained by Echeverría et al. (2013) in the western sector of the EBSZ as well as with the deformation rates previously obtained from displaced geomorphic and stratigraphic markers.

The main objective of this study is to determine deformation rates using episodic GPS observations from the eastern end of the EBSZ and to interpret these data within the regional tectonic setting of the Western

Mediterranean area. Our data and interpretations will significantly increase our knowledge of the active tectonics of one of the areas with the highest seismic activity in Spain and will be the basis for multiple ongoing studies intending to improve the seismic hazard of this populated region.

## 2. Regional Geodynamic Setting

The Bajo Segura Basin (Eastern Betic Cordillera; Figure 1) is located on the diffuse plate boundary between Africa and Eurasia. These plates converge at a rate of approximately 4 to 6 mm/year in the NW-SE direction (see review by Nocquet, 2012, and Sella et al., 2002; McClusky et al., 2003; Fernandes et al., 2007; Serpelloni et al., 2007; DeMets et al., 2010; Koulali et al., 2011; Argus et al., 2011). This plate convergence is responsible for the NNW-SSE compressive tectonic regime in the Eastern Betic Cordillera (Galindo-Zaldívar et al., 1993; Montenat et al., 1990; Oláiz et al., 2009).

Within this convergent geodynamic setting is the EBSZ (Figure 1), a left-lateral tectonic corridor extending between Almería and Alicante (Bousquet, 1979; De Larouzière et al., 1988; Silva et al., 1993). The strikes of these active faults (i.e., the Carboneras, Palomares, Alhama de Murcia, Hinojares, Los Tollos, Carrascoy, Crevillente, and Bajo Segura faults) progressively grade from NNE-SSW to NE and then to ENE-WSW in the study area. The Bajo Segura Basin is located at the northern onshore end of this shear zone.

Several studies have estimated that most of the present-day plate convergence is accommodated in northern Africa and that the rest must be transferred and accommodated northward. According to Serpelloni et al. (2007), between 2.7 and 3.9 mm/year of the present-day plate convergence is accommodated in the Algerian Tell, and active shortening must occur at rates ranging from  $1.6 \pm 0.6$  to  $2.7 \pm 0.6$  mm/year across the Algero-Balearic Basin and the SE Iberian Peninsula (Eastern Betic Cordillera). Pérez-Peña et al. (2010) estimated that an average velocity of  $\sim 2.3$  mm/year occurs in a N-S direction in the eastern region of the Iberian Peninsula. Echeverría et al. (2013) estimated that the velocities within the EBSZ range from 1 to 3 mm/year with respect to Eurasia and that 3 to 4 mm/year of deformation is most likely concentrated in northern Africa. Palano et al. (2013) estimated that a compressional regime exists in the study area in a NW-SE direction. Palano et al. (2015) postulated that shortening in the Eastern Betic Cordillera is the result of the partial transfer of the overall plate convergence related to an indenter located to the northwest of Algeria.

Other regional studies have provided contradictory results for the study area due to the scarcity of GPS sites available at the NE end of the EBSZ. Stich et al. (2006) indicated that the northern part of the EBSZ comprises a transtensional regime with N-S shortening and ENE-WSW extension. Fernandes et al. (2007) indicated that the ALAC site (the permanent GPS site located in the NE region of our study area) is located in a stable area. These results are not in agreement with the local geology, which is characterized by active transpression (Alfaro et al., 2012; Silva et al., 1993).

## 3. Deformation of the Bajo Segura Basin: Previous Results

The Bajo Segura Basin is bordered to the north by the CF (Figure 1; Martín-Rojas et al., 2015) and to the south by the Bajo Segura Fault Zone (Alfaro, Andreu, et al., 2002; Alfaro, Delgado, et al., 2002; Montenat et al., 1990; Silva et al., 1993). The orientations of both active faults, which are roughly perpendicular to the maximum horizontal compression, explain the sinistral-reverse kinematics of the ENE-WSW CF and the reverse kinematics of the E-W Bajo Segura Fault.

### 3.1. CF (Abanilla-Alicante sector)

The CF (Abanilla-Alicante sector) characterizes the northern limit of the Bajo Segura Basin (Figure 1, Martín-Rojas et al., 2014, 2015). This fault is a key structure in the recent evolution of the Eastern Betic Cordillera, as it represents the former limit between the two continental plates that collided during the Miocene to form the Betic orogenic belt (Martín-Algarra & Vera, 2004; Sanz de Galdeano, 1983, and references therein). During this collision, the CF was a dextral strike-slip fault. However, after the Upper Miocene, geological data such as drag folds, progressive unconformities and slickenlines have indicated that the CF exhibits reverse-sinistral kinematics as a result of the regional tectonic setting (Alfaro et al., 2012; Alfaro, Delgado, et al., 2002).

The CF is considered an active fault (Alfaro, Andreu, et al., 2002; Alfaro, Delgado, et al., 2002; Bousquet, 1979; De Larouzière et al., 1988; García Mayordomo, 2005; Gauyau et al., 1977; Martin-Rojas et al., 2015; Silva et al., 1993; Silva et al., 2003); this fault is included in the Quaternary Active Faults Database of Iberia (IGME, 2015). Evidence of Quaternary deformation includes rare deformed deposits of probable Quaternary age (Martin-Rojas, 2015), geomorphic features (Goy & Zazo, 1989; Silva et al., 1993), uplifted Tyrrhenian marine terraces (Bousquet, 1979; Goy et al., 1993) and seismites (Alfaro et al., 1999) (see Martin-Rojas et al., 2014 for further discussion). The vertical slip rates proposed for the CF derived from displaced stratigraphic and geomorphic markers range from 0.01 up to 0.07 mm/year (García Mayordomo, 2005; Goy & Zazo, 1989; Silva et al., 2003; Soria et al., 2001).

The CF continues to the west of the Bajo Segura Basin. In its western sector (Murcia province), several significant earthquakes have occurred in the last two decades along or next to its trace (i.e., the 1999 Mula, 2002 Bullas, and 2005 Zarcilla de Ramos-La Paca earthquakes, with a magnitude of approximately 5).

### 3.2. Bajo Segura Fault Zone

The Bajo Segura Fault Zone (BSFZ) characterizes the southern limit of the Bajo Segura Basin (Figure 1; Montenat, 1977). This structure is characterized by a set of ENE-WSW-trending blind thrust faults that offset the Triassic basement and are responsible for the active folding of the Upper Miocene-Quaternary sedimentary cover. The main active structures of this fault zone are two ENE-WSW-striking reverse blind faults, the Torremendo and Bajo Segura Faults, and several secondary NW-SE-striking dextral faults (the San Miguel de Salinas, Torreveja, and Guardamar Faults). These structures continue offshore eastward (Alfaro, Delgado, et al., 2002; Perea et al., 2012).

The BSFZ shows the most prominent geologic and geomorphic evidence of active tectonism in the Bajo Segura Basin (Alfaro et al., 2012; Alfaro, Andreu, et al., 2002; Alfaro, Delgado, et al., 2002; García-Mayordomo & Martínez-Díaz, 2006; Montenat, 1977; Taboada et al., 1993). Folding and reverse faulting have accommodated shortening onshore (Bousquet, 1979; Silva et al., 1993; Alfaro, Andreu, et al., 2002; Alfaro et al., 2012) and offshore (Alfaro, Delgado, et al., 2002; Maillard & Mauffret, 2013; Perea et al., 2012). The BSFZ has also exhibited intense seismic activity during historical and instrumental periods (Giner et al., 2003). This fault zone is the most likely seismogenic source of the 1829 Torreveja earthquake ( $MSK = X$ ;  $M_s = 6.3-6.9$ ) and the 1919 Jacarilla-Torremendo composite earthquake ( $M_w=5.5$ , Batlló et al., 2015). Moreover, this area presents the highest seismic hazard in Spain (Seismic Hazard Map of Spain; IGN, 2015).

Geological and geomorphological data point to fault slip rates ranging from 0.2 to 0.4 mm/year (Alfaro et al., 2012; Alfaro, Andreu, et al., 2002; García-Mayordomo & Martínez-Díaz, 2006; Giménez et al., 2009). These data are also consistent with the results estimated by a high-precision leveling profile that is 30 km long (27-year span), which indicates uplift rates of 0.2 mm/year related to the Bajo Segura Fault (Giménez et al., 2009). Higher fault slip rates, ranging from 0.75 to 1 mm/year, have also been reported (Taboada et al., 1993). However, these values are based on the misinterpretation of the marker age used (see discussion in Alfaro et al., 2012). According to the estimated maximum rupture dimensions and the empirical relationship proposed by Stirling et al. (2002), the BSFZ could produce earthquakes with maximum estimated magnitudes ( $M_w$ ) ranging from 6.6 to 7.1, with approximate recurrence intervals ranging from 4.500 to 21.500 years (Alfaro et al., 2012).

## 4. GPS Data and Results

### 4.1. GPS Network of the Bajo Segura Basin

A GPS network with 11 geodetic quality control points was installed to provide coverage of the main active faults in the region (Figure 1B). The GPS monuments (named 7001–7011) were built using concrete with steel rebar over bedrock at a depth of 50 cm to guarantee the stability and reliability of the results. Sites 7002 to 7005 allow to estimate slip rates related to the CF, while sites 7006, 7007, and 7009 to 7011 provide deformation rates along the BSFZ. Sites 7001 and 7008 are located to the north and south of the Bajo Segura Basin, respectively, and they occur over the outcropping basement of the basin. Site 7004 was not considered in our analysis as the monument was partially destroyed.

Several permanent GPS stations were set up by the Instituto Geográfico Nacional de España (Spanish Geographical Survey) during the time span of our analysis. We considered to include data from these

permanent stations in our study. However, these stations are located in a pier (ALAC, Alicante station) or in building rooftops (Abanilla ABAN and Torrevejeja TORR). Moreover, all these antennas are placed at the top of ~3-m-long steel poles fixed with iron cords. Consequently, we carried out a previous detailed study of noise sources in the GPS time series to evaluate if these sites are compatible with the standards of a geodynamic-geodetic analysis. The results showed that all the permanent stations considered present values of white noise around 1 mm per component. In addition, the values of random walk noise are higher than  $2.5 \text{ mm}/\sqrt{\text{year}}$ . Several studies considered random walk values of  $1 \text{ mm}/\sqrt{\text{year}}$  (Beavan et al., 2016; Shen et al., 2011, among others) or even lower (Echeverria et al., 2013). Consequently, we postulate that this high random walk noise is related to monument instabilities. So, we consider that the permanent stations are not suitable to measure the small deformation values of the area.

#### 4.2. GPS Data and Processing

The results presented here are based on four episodic GPS campaigns conducted during a 13-year time span (June 1999, September 2001, September 2002, and January 2013; Sánchez-Alzola et al., 2014). These campaigns were conducted in the summer (June and September), except for the last campaign, which was conducted in the winter (January), and used accurate self-centering mounting devices to guarantee that the GPS observations were obtained from the same planimetric position during each geodetic campaign. The sites were observed for a minimum period of 8 hr a day during 2 or 3 days in the old campaigns (1999, 2001, and 2002) but increasing to a continuous 96-hr interval in the last campaign.

GPS data were processed using version 6.2 of the GIPSY-OASIS software developed at the NASA Jet Propulsion Laboratory (<https://gipsy-oasis.jpl.nasa.gov/>). This package uses a zero-difference ambiguity resolution to compute PPP with the gd2p.pl module. This program processes dual-frequency GPS data from single-receiver observations to estimate the wide lane and phase bias from the global network of GPS stations. The processing method is described as follows. The episodic GPS observations were processed with the GIPSY-OASIS (GOA) gd2p.pl module using the methodology described in Bertiger et al. (2010). This module was invoked with the flags set for ocean loading, ambiguity resolution, receiver antenna absolute phase centers, ephemeris and Earth orientation files, total electronic content estimation, tropospheric delays, and elevation masks necessary to process episodic observations. GOA software accesses all of the auxiliary files required for the PPP process, such as precise ephemeris, clock files, and antenna phase calibration files, and it downloads them from its own FTP server ([ftp://sideshow.jpl.nasa.gov/pub/JPL\\_GPS\\_Products/Final](ftp://sideshow.jpl.nasa.gov/pub/JPL_GPS_Products/Final)). The GPS solutions were computed in a homogenous IGS08 global reference frame since the last GIPSY-OASIS product reprocessing, which was performed in 2011 (Desai et al., 2011). To obtain the position time series for the entire period of the campaigns, all GPS observations were processed with an identical standard PPP procedure using the Jet Propulsion Laboratory final ephemeris and Earth orientation products. To model atmospheric delays, the hydrostatic and wet components of the zenith tropospheric delay were calculated. Likewise, we considered the total electronic content values based on the International Reference Ionosphere (Bilitza, 2001). We did not employ second-order ionosphere corrections in this processing. The ocean tidal loading model FES2004 (Lyard et al., 2006) from the Onsala Space Observatory was applied (<holt.oso.chalmers.se/loading>). Furthermore, to avoid multipath effects and improve the velocity assessment, an elevation mask of  $10^\circ$  and a 30-s processing sampling were used for the coordinate estimation. We employed the latest IGS08\_week.ATX antenna calibration file to correct the Antenna Phase Centre. Eventually, with the use of the PPP technique, no network adjustment was applied, and only daily solutions were considered.

Once the data from all 11 control points from all observation campaigns were processed, we generated the position time series by transforming the raw geocentric coordinates into their horizontal components (east and north). Figure 2 shows the detrended position time series for the 11 GPS points of the Bajo Segura geodetic network in both horizontal directions (i.e., east and north). This paper does not address vertical deformation rates since the analyzed campaign-style GPS velocities do not provide sufficient resolution.

To improve velocity estimations, the obtained time series were inspected and filtered with a rough outlier estimation based on a  $2.5\sigma$  standard deviation threshold from the detrended time series. All the points outside this interval were considered outliers and were not included in the linear regression calculation. Hence, no offsets or jumps due to unreliable observations were included. To model geophysical processes, such as plate tectonics and surface deformation, it is necessary to obtain long time intervals of station motion to

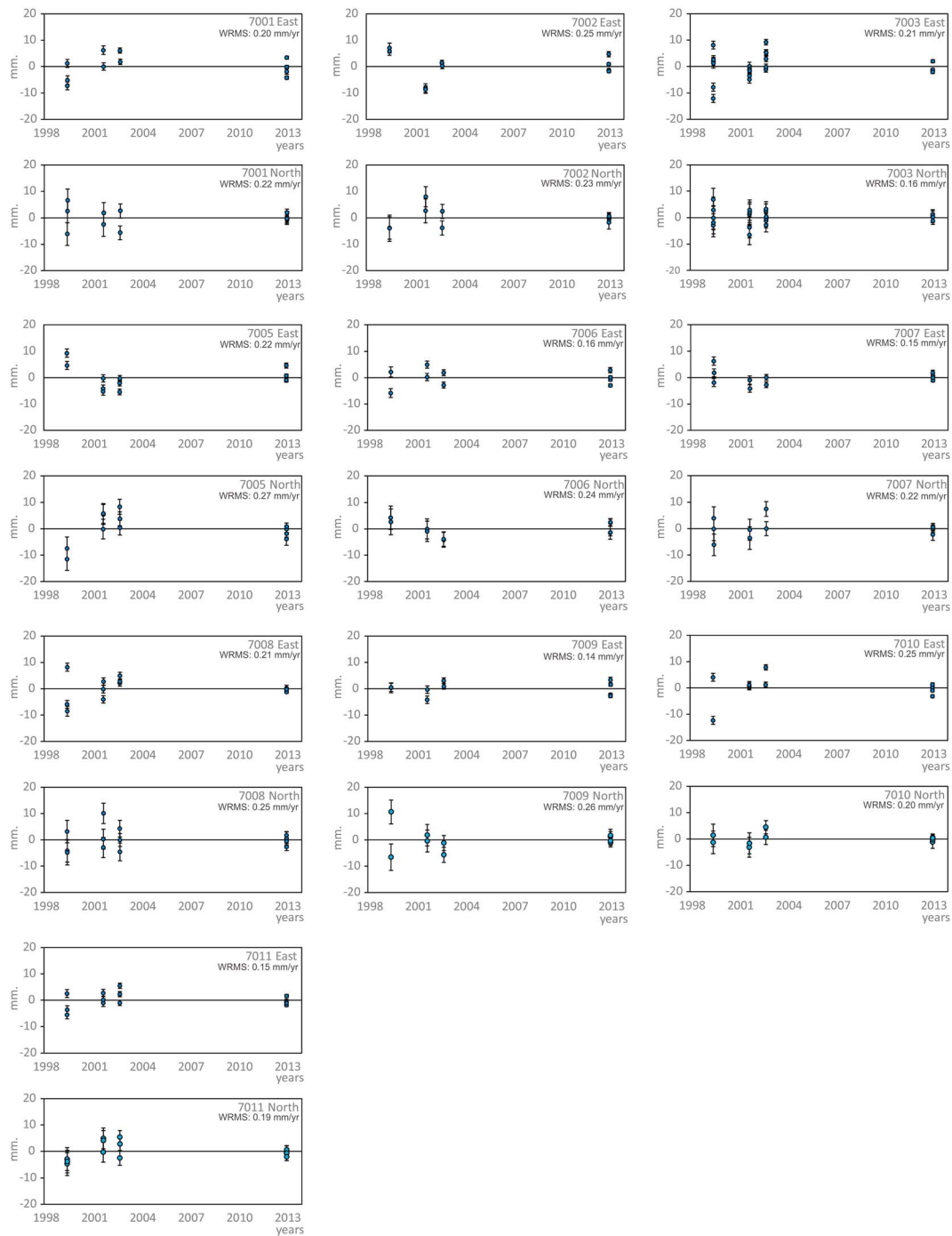


**Figure 2.** Detrended position time series of the Bajo Segura Basin GPS sites. Time series computed with GISPY-OASIS software in IGS08b reference frame using a linear regression fit to detrend. WRMS error of each component in millimeters are also included. The north and east components and the error bars are in millimeters.

enhance velocity estimations; using a 13-year time interval of GPS observations from this network allowed us to minimize the effects of white noise and periodicity in the velocity estimation with realistic error bounds.

### 4.3. Velocity Field

We first assumed a linear node to best fit the trend line to the time series of the positions for each station using linear regression. It was done to compute the velocity field and 95% confidence error bounds. Due

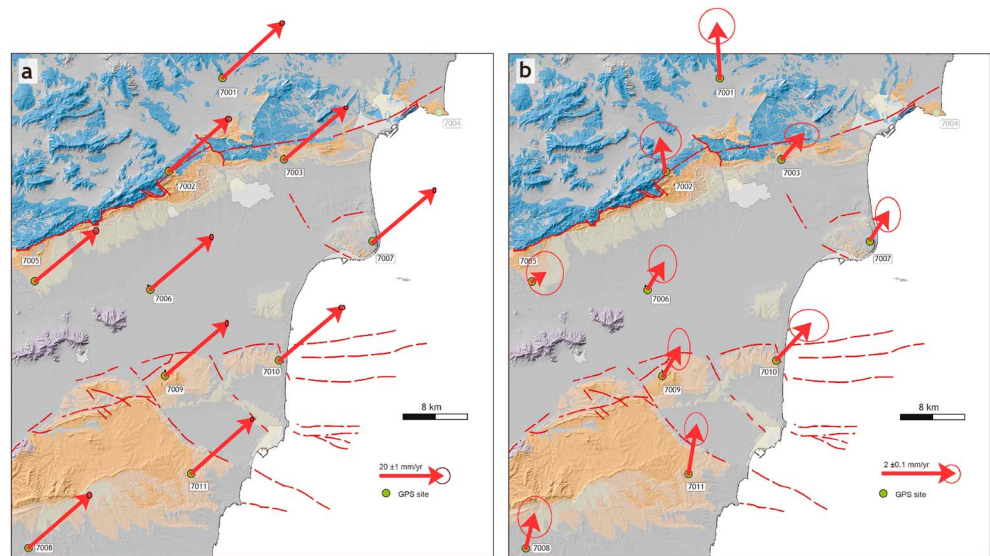


**Figure 3.** Bajo Segura GPS network absolute velocity field in IGS08b reference frame derived from time series (a) and residual velocity field estimated with respect to stable Eurasia as defined by the ITRF2008 plate motion model (Eurasia-fixed reference frame) (b). Magnitudes are in millimeter per year with 95% confidence error ellipses, assuming white noise and random walk noise error model. Legend as in Figure 1b.

to the sparse amount of data obtained from a 13-year timespan without a continuous record, no periodicity was introduced into the velocity estimation. The error model for our episodic data can be represented by a combination of white noise and random walk noise. Here we assume a random walk noise value of  $1 \text{ mm}/\sqrt{\text{year}}$  as in the analysis of other campaign GPS sites (Beavan et al., 2016; Shen et al., 2011). Figure 3A shows the present-day GPS-derived absolute velocity vectors and 95% confidence error ellipses obtained here. Our PPP solutions are also compared with the ITRF2008 plate motion model (using the transformation parameters defined in Altamimi et al., 2012) to obtain a residual velocity field (Table 1, Figure 3B). We use the Eurasian Plate transformation parameters of the ITRF2008 plate motion model with the geographical coordinates of our points as inputs. We assume that the stations belong to a nondeforming block and rotate the velocity solution into a Western Europe reference frame. We chose this reference frame because we think that this is the best option for the regional implications of our data on the diffuse plate boundary

**Table 1**  
*East and North Absolute Velocities Estimated for the Bajo Segura GPS Network*

Sites	Coordinates		Residual velocities									
			IGb08 absolute velocities				ITRF2008 PMM Eurasia fixed			N70E projection		
	Lat. (°N)	Long. (°W)	$V_E$	$V_N$	$\sigma_E$	$\sigma_N$	$V_E$	$V_N$	$V_{\text{mod}}$	Parallel	Normal	
7001	38.4050	-0.7340	19.79	18.13	0.20	0.22	-0.08	1.54	1.54	0.45	1.48	
7002	38.3000	-0.8133	19.74	17.53	0.25	0.23	-0.15	0.94	0.95	0.18	0.93	
7003	38.3106	-0.6446	20.51	17.30	0.21	0.16	0.60	0.71	0.93	0.80	0.46	
7005	38.1757	-1.0136	20.23	16.83	0.22	0.27	0.35	0.23	0.42	0.41	0.09	
7006	38.1651	-0.8469	20.34	17.30	0.16	0.24	0.43	0.70	0.82	0.64	0.51	
7007	38.2086	-0.5171	20.46	17.36	0.15	0.22	0.50	0.77	0.92	0.74	0.55	
7008	37.8705	-1.0300	20.18	17.56	0.21	0.25	0.23	0.95	0.98	0.54	0.81	
7009	38.0673	-0.8250	20.40	17.42	0.14	0.26	0.47	0.82	0.95	0.72	0.61	
7010	38.0759	-0.6588	20.91	17.61	0.25	0.20	0.95	1.02	1.39	1.24	0.63	
7011	37.9499	-0.7912	20.19	17.95	0.15	0.19	0.22	1.35	1.37	0.67	1.20	

*Note.* Deviations are computed based on linear regression adjustment. Residual local horizontal velocities are calculated with respect to the ITRF2008 plate motion model (Altamimi et al., 2012) Eurasia-fixed. Parallel and normal residual velocities are projected along the Crevillente Fault trace (azimuth N70E). All values are in millimeter per year.

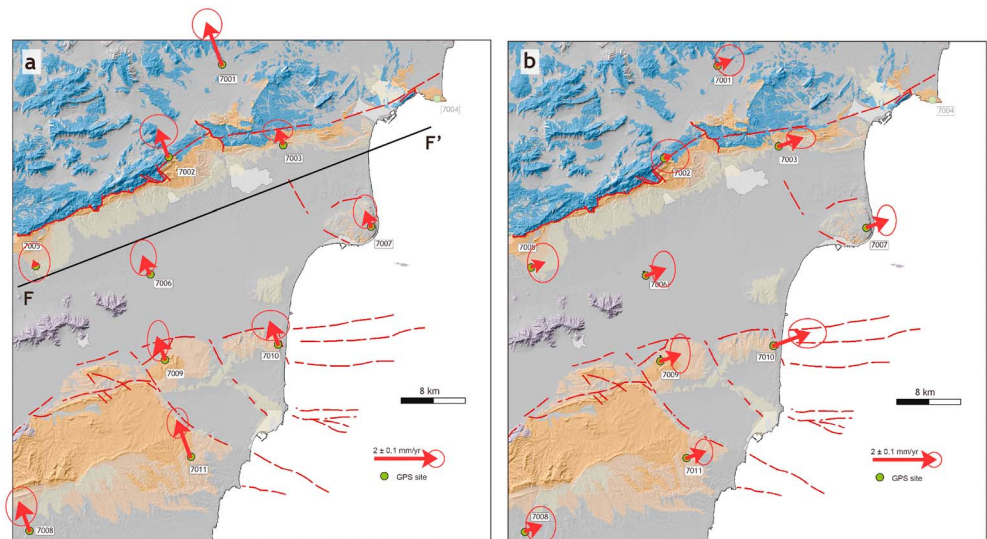


**Figure 4.** Bajo Segura GPS network residual velocities field projected parallel (a) and normal (b) to profile FF' (N70E direction). Residual velocity field is estimated with respect to stable Eurasia as defined by the EUR pole of rotation estimated by Altamimi et al. (2012). Magnitudes are in millimeter per year and 95% confidence error ellipses, assuming white noise plus random walk noise error model. Legend as in Figure 1b.

of the Nubian and Eurasian plates (see section 5.3 below). We also compute the N-S (N) and E-W (E) components of the residual velocity vectors (Table 1). We postulate that the use of alternative reference frames to obtain residual velocities will not significantly change the general deformation pattern of the study area (see below) because, as we are dealing with a local network (less than 70 km long), such a change will homogeneously affect all the displacement vectors of the network.

The Bajo Segura network GPS-derived velocities in a Western Europe reference frame (Figure 3b) exhibit two main directions. The velocity vectors located to the south of the CF (sites 7003 to 7011) are directed to the NE (with magnitudes ranging from 0.4 to 1.4 mm/year). The two sites located to the north of the CF (sites 7001 and 7002) are directed to the NNW (with magnitudes ranging from 1.0 to 1.5 mm/year). Within the southern group of sites, a general decrease in northward velocity can be observed. Similarly, in the northern group of stations, a slight decrease in velocity is also observed.

To quantify the strike-slip kinematics of the CF (see below), we also study the transect F-F' (N70E direction), which coincides with the trace of this fault. We generate parallel and normal IGS08 residual velocities using these directions. Table 1 shows the absolute velocities obtained in the IGS08 reference frame with their 2.5 standard deviations, the residual velocities obtained with respect to the ITRF2008 plate motion model, and their parallel and normal projections to the mean direction of the CF (N70E). Figure 4 includes the parallel velocity vectors computed from the F-F' transect projection (azimuth N70E). Figure 5 presents the parallel and normal velocities of the F-F' profile with  $1\sigma$  uncertainties. We observe statistically significant (at 95% confidence level) differential motion between the stations located to the north and south of the CF, reflecting a velocity offset (i.e., slower motion to the north of the CF).

## 5. Discussion

These results obtained from the Bajo Segura GPS network aid in a better definition of the kinematics of the Eastern Betic Cordillera and provide significant local and regional conclusions about the tectonic setting of this region. The main issue with the GPS-derived residual velocities used in our interpretation is that they are quite small (submillimeter) but are clearly nonzero at the 95% confidence level. Our results are in good accordance with geodetic data and models previously published in the literature, as well as with the geological observations obtained at regional and local scales (see below). We discard data from site 7005 in our analysis, as the obtained residual velocity is not significant at 95% confidence (Figure 3).



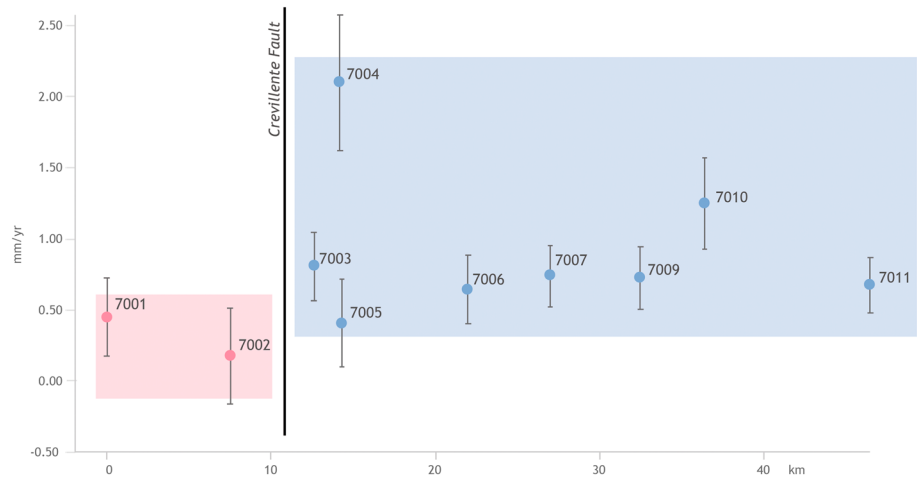


**Figure 5.** F-F' profile (azimuth N70E) parallel residual velocities along a profile normal to fault strike (azimuth N160E) with error bars ( $1\sigma$ ). Blue and red points represent stations located to the south and north of the CF, respectively. Station 7004 has been excluded from the analysis and the calculation of the average of the stations north of CF. Note the velocity offset indicating differential motion between stations located to the south and north of the CF.

## 5.1. Fault Kinematics and Partitioning of Deformation in the Bajo Segura Basin

### 5.1.1. CF

We interpret the GPS-derived velocities described above in terms of the CF and BSFZ kinematics to propose deformation partitioning in the Bajo Segura Basin. We calculate the F-F' parallel component of motion by subtracting the residual velocities of the stations located to the North and South of the CF. We obtained a value for this parallel component of  $V_{FF} = 0.8 \pm 0.2$  mm/year (Figure 3 and Table 1). This value is greater than zero at 95% confidence level; hence, it indicates that, at present, the CF presents a sinistral strike-slip component in agreement with surface geological data (Montenat, 1977). The derived velocity, however, is calculated using a single site on the northern side of the CF; consequently, this preliminary interpretation may not represent the uniform motion occurring along the entire fault. These GPS data represent the first quantitative fault slip rates attributed to the CF. In the CF, no previous short-term accurate fault slip rates based on geological or geomorphological markers have been previously reported.

This GPS-derived strike-slip rate is lower than those obtained by Echeverria et al. (2013, 2015) in the central and SW sectors of the EBSZ (CuaTeNeo GPS network). These authors estimated left-lateral slip rates of  $1.3 \pm 0.2$  mm/year for the Carboneras fault (SW of the EBSZ) and  $1.5 \pm 0.3$  mm/year for the Alhama de Murcia fault (in the central part of the EBSZ; Figure 6). These first geodetic results of the Bajo Segura GPS network must be confirmed in future GPS studies. The decrease in left-lateral displacement observed in our study area, which is located at the NE end of the EBSZ, could be related to the change in strike of this regional tectonic corridor, which is NE-SW in the central region (i.e., oblique to the regional maximum compressive stress characterized by SHmax NNO-SSE; Galindo-Zaldívar et al., 1993) and ENE-WSW in our study area (i.e., roughly perpendicular). Similarly, the normal component resolved across the CF trace seem to point to apparent extension related to this structure (mean  $V_{FF} = -0.7 \pm 0.2$  mm/year; Table 1 and Figure 4). This apparent extension is not in agreement with geological data, as no significant extensional structures have been reported in this area. In contrast, shortening-related structures (i.e., folds, thrusts, and reverse faults) are abundant (Montenat, 1977; Martín-Rojas et al., 2015, among many others). This disagreement is hard to explain, so we postulate that further analyses are necessary to better constrain both regional geology and geodetic data. A possible explanation could be a very recent change in the local tectonic regime of this area, which is recorded by the GPS signal but has not produced a geological imprint yet.

### 5.1.2. Bajo Segura Fault Zone

In the BSFZ, the north components of velocity vectors permit the analysis of the deformation of the fault zone along its strike (Figure 3 and Table 1). The shortening rates computed using the N velocity

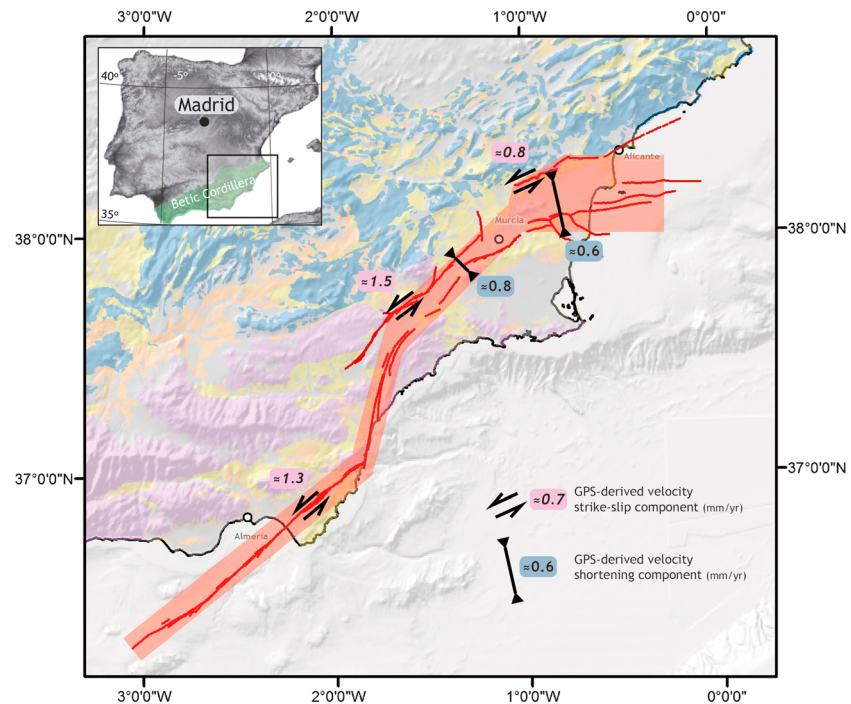


**Figure 6.** Shortening and strike-slip GPS-derived slip rates for the Eastern Betic Shear Zone (EBSZ). Left-lateral displacement rate decreases in our study area with respect to the central EBSZ, probably because of the change in strike of this regional tectonic corridor (approximately N45E in the south and central sectors and N70E to ~N-S in the study area). Data to the west of the Bajo Segura Network after Echeverria et al., 2013, 2015). Legend as in Figure 1a.

component are  $V_N = 0.7 \pm 0.2$  mm/year in the western sector,  $V_N = 0.6 \pm 0.2$  mm/year in the central sector, and  $V_N = 0.3 \pm 0.25$  mm/year in the eastern sector. These values seem to indicate an eastward decrease in shortening along the strike of the BSFZ, although we cannot rule out that this could be an artifact related to the low signal-to-noise ratio observed at the 95% confidence level. However, this interpretation is consistent with geological observations, as N-S strain (deduced based on the tightness of fault propagation folds) also decreases in the same direction (Alfaro et al., 2012).

GPS data indicate a mean shortening rate related to the BSFZ of  $0.6 \pm 0.2$  mm/year, which is consistent with the geological fault slip rates estimated for the BSFZ. Alfaro et al. (2012), using stratigraphic and geomorphic markers, estimated long-term fault slip rates varying between 0.2 and 0.4 mm/year. Previous authors reported higher slip rates (0.75 and 1 mm/year; Taboada et al., 1993), but later chronostratigraphic precision of the marker used in this study yielded a slip rate within the range proposed by Alfaro et al. (2012). Geological observations indicate that the BSFZ presents a major reverse component (Alfaro et al., 2012; Montenat, 1977, and references therein), but no direct data about fault kinematics have previously been reported, as it is a blind fault. All of the present-day GPS-derived residual velocity vectors related to the BSFZ indicate its NE direction of motion, even when considering the uncertainties (expressed as error ellipses at the 95% confidence level in Figure 3B) and the fact that the stations located to the north of the BSFZ show lower velocities than the stations located to the south of the fault, as previously discussed. As the fault zone strikes ENE-WSW, the orientation and module of the velocity vectors seem to point to an oblique reverse-sinistral kinematics of the BSFZ. This finding is in agreement with the kinematics of the Carrascoy Fault deduced based on surface geological observations (Martin-Banda et al., 2016); this fault is located along the EBSZ in the western extension of the Bajo Segura Fault (Figure 1).

The fault-normal shortening rate related to the BSFZ (Figure 6) seems to be statistically lower or equal in our study area ( $0.6 \pm 0.2$  mm/year) than it is in the central part of the tectonic corridor ( $0.8 \pm 0.2$  mm/year; Echeverria et al., 2013). If this shortening is actually lower, it could be related to the existence of some

active structures to the north and/or south of our study area, that is, outside the EBSZ, which accommodates part of the deformation in this region (see below).

### 5.2. Southward Migration of Shortening in the Bajo Segura Basin

We analyze in this section N components of the GPS-derived velocities to investigate how the regional N-S shortening (related to the regional compressive tectonic regime) is distributed along the Bajo Segura Basin. These N components (normal to the general trend of the BSFZ) point to a heterogeneous distribution of shortening along the Bajo Segura Basin (Figure 3 and Table 1). Our data indicate that in the southern sector of the basin, the mean N shortening rate is  $V_N = 0.6 \pm 0.2$  mm/year. In the northern sector of the basin, to the south of the CF, the shortening is almost zero ( $V_N = 0.06 \pm 0.15$  mm/year). These values seem to indicate a N-S shortening gradient along the Bajo Segura Basin, which is lower in the northern sector and increases to the south. However, again, these values fall within the range of their computed errors; thus, the confirmation of this hypothesis requires further data. We postulate that the present N-S shortening is mainly accommodated in the south of the basin, along the BSFZ. Geological evidence seems to indicate that the maximum uplift (related to shortening) of the CF occurred during Messinian times and decreased during the Pliocene and Quaternary (Martin-Rojas et al., 2015). Combining these geological data with the above-described geodetic data indicates the southward migration of the main deformation (shortening) area, which was located in the northern part of the basin during the Upper Miocene and is presently located in the southern sector.

### 5.3. Implications for the Diffuse Plate Boundary of the Nubian and Eurasian Plates

Regional GPS studies of the Nubia-Eurasia plate boundary have estimated that most present-day plate convergence is accommodated in northern Africa and that the remaining convergence must be transferred and accommodated northward (Echeverria et al., 2013; Pérez-Peña et al., 2010; Serpelloni et al., 2007). The estimated residual shortening (ranging from 1.6 to 2.7 mm/year, according to the authors mentioned above) must be accommodated across a wide area, including the Algero-Balearic Basin and the Eastern Betic Cordillera in southern Spain (Serpelloni et al., 2007). However, regional GPS studies (Pérez-Peña et al., 2010; Serpelloni et al., 2007) have not related these data to specific faults due to their low density of GPS sites.

Studies of active tectonics indicate that the EBSZ (Figures 1 and 7) is the main onshore tectonic structure accommodating the NNW–SSE plate convergence in the Eastern Betic Cordillera (Alfaro et al., 2012; De Larouzière et al., 1988; Martin-Banda et al., 2016; Martínez-Díaz et al., 2012; Masana et al., 2004; Silva et al., 1993). Our GPS study, which is located at the NE end of the EBSZ, shows that the mean shortening rate in the Bajo Segura Basin is  $0.6 \pm 0.2$  mm/year. These shortening values are consistent with those obtained by the CuaTeNeo GPS network (Echeverria et al., 2013) in the central part of the EBSZ (Figure 6; Echeverria et al., 2013, 2015), where the estimated shortening rate is  $0.8 \pm 0.4$  mm/year in the N315E direction. Consequently, our GPS data, together with those published by Echeverria et al. (2013), indicate that despite the low signal-to-noise ratios, the EBSZ accommodates a significant fraction (~25%, i.e.,  $0.6\text{--}0.8 \pm 0.4$  mm/year) of the overall convergence in the Eastern Betic Cordillera and Mediterranean Sea (between 1.6 and 2.7 mm/year according to Serpelloni et al., 2007, or approximately 2 mm/year according to Pérez-Peña et al., 2010). Nevertheless, another significant part must be accommodated to the north (the External Zone of the Eastern Betic Cordillera) or to the south (the Cartagena Basin and its neighboring offshore area) of the EBSZ. No significant instrumental seismicity has been recorded in the wide sector of the Mediterranean Sea located to the south of our study area (Figure 7). Because the rheology of this anomalous crust resists deformation, it is likely that this Mediterranean sector does not accommodate major deformation. In contrast, the occurrence of seismic activity in the External Zone of the Betic Cordillera, to the north of the EBSZ (e.g., the 1748 Estubeny, 1644 Muro de Alcoy, 1396 Tavernes, and 2017 Caudete earthquakes; Figure 7) confirms that the region is still active. In addition, there is geological evidence of relevant active structures to the south of the EBSZ, that is, in the Cartagena Basin and the onshore area next to Cartagena (see active faults in QAFI; IGME, 2015). As a consequence, we hypothesize that the fraction of overall convergence between Nubia and Eurasia that is not accommodated in North Africa is mainly distributed onshore in the Eastern Betic Cordillera (in the EBSZ and to the south and north of this tectonic corridor) and offshore, adjacent to the Spanish coast (south of the Cartagena Basin), but not in the central part of the Mediterranean Sea (the Algero-Balearic Basin).

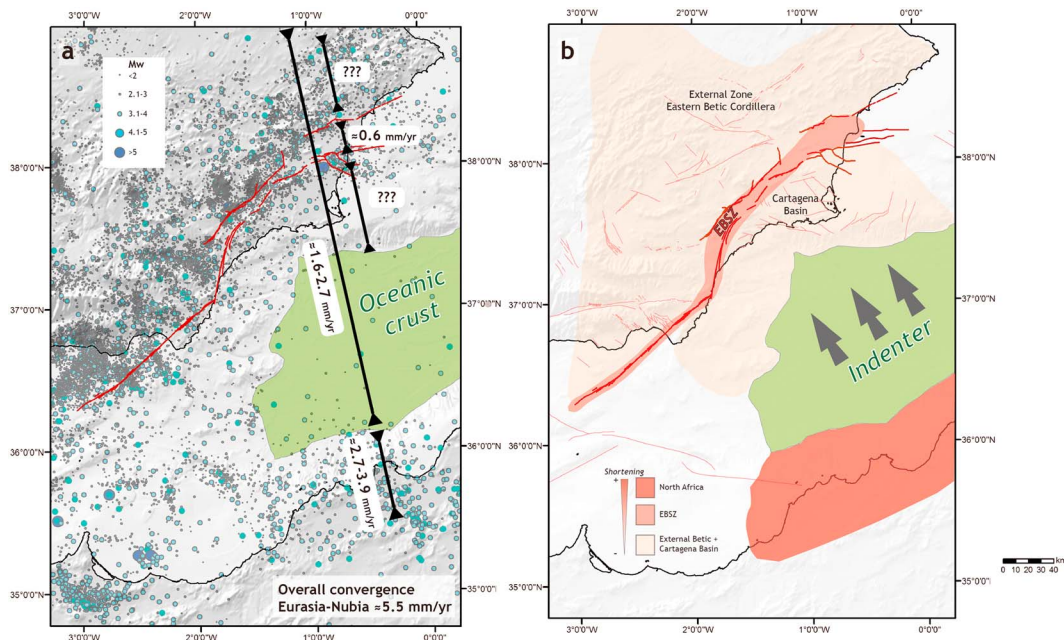


**Figure 7.** (a) Map of the eastern sector of the Nubia-Eurasia plates. The anomalous crust of the Argero-Balearic Basin is shown in green (oceanic crust, according to Booth-Rea et al., 2007). The thick black lines represent the fractions of regional GPS-derived plate convergence. The thin lines represent the partial local GPS-derived shortening rates. Question marks indicate areas with no GPS data. Circles represent historical and instrumental seismicity ( $M_w > 2$ ). (b) Same area as Figure 7a. Again, the oceanic crust of the Argero-Balearic Basin is shown in green. We postulate that this oceanic crust does not accommodate significant deformation. We interpret the oceanic crust as the rigid indenter hypothesized by Palano et al. (2015), which is responsible for the transfer of the Nubia plate convergence to the Eastern Betic Cordillera. In this sector, most deformation is concentrated along the Eastern Betic Shear Zone (EBSZ), but part of the overall convergence should also be accommodated to the north and south of this tectonic corridor. The Alboran Basin, which is located to the west of the oceanic crust, is characterized by continental (and magmatic arc-like) crust, which is not rigid enough to transfer the convergence to the Central Betic Cordillera.

The geodynamic regime of the Western Mediterranean region is dominated by the NW-directed convergence between Nubia and Eurasia (Nocquet, 2012, and references therein). Different hypotheses involving different lithospheric blocks have been postulated within this regional tectonic setting. Vernant et al. (2010) presented a model involving two additional blocks independent of both Nubia and Eurasia. Koulali et al. (2011) postulated a model containing one block between Eurasia and Nubia, including the SW Betics, the Alboran Sea, and the Central Rif. Palano et al. (2015) postulated the existence of an indenter located at the northern limit of the Nubian plate, which transferred a fraction of the convergence rate into the Eastern Betic Cordillera. We consider that the model of Palano et al. (2015) best explains the geological observations, seismicity, and detailed GPS data recently obtained from local networks (Echeverria et al., 2013, 2015, and data presented in this work). Geological, seismological, and geodetic data indicate that the central and Eastern Betic Cordillera are two different tectonic domains (De Larouzière et al., 1988; Echeverria et al., 2013, 2015; Galindo-Zaldívar et al., 2015; Silva et al., 1993, among many others). Presently, the central sector is dominated by extension, while the eastern sector is dominated by oblique strike-slip and reverse tectonics along the EBSZ.

The onshore limit between the two abovementioned tectonic domains (Figure 7) is aligned with the estimated limit between the anomalous crust (which is oceanic, according to Booth-Rea et al., 2007) of the Argero-Balearic Basin and the thin continental (and magmatic arc-like) crust of the Alboran Basin (Booth-Rea et al., 2007; Comas et al., 1999). We postulate that this rigid and resistant crust acts as the indenter proposed by Palano et al. (2015) and is probably responsible for the present deformation of the EBSZ. This indenter is responsible for the two different tectonic domains presently recognized in the central and Eastern Betic Cordillera. In the eastern sector, the rigid anomalous crust of the Argero-Balearic Basin (Booth-Rea et al., 2007) transfers the convergence of the Nubian and Eurasian plates, producing deformation in this tectonic domain.

The higher values of fault slip rates obtained in the eastern and central sectors of the EBSZ (Echeverría et al., 2013, 2015) compared with those obtained in our study area (at the NE end of the EBSZ) could be related to the presence of the Cartagena Basin and its neighboring offshore area between the left-lateral tectonic corridor and the indenter.

#### 5.4. Alternative Interpretation of Residual Velocities

The GPS-derived residual velocities we obtained are very small relative to zero with large errors. Consequently, they could also be interpreted as an evidence of no active tectonics in the study area. However, several lines of evidence clearly indicate that this area is tectonically active. The Bajo Segura Basin is considered an area of higher seismic hazard in the Iberian Peninsula (IGN, 2015). In fact, continuous instrumental seismic activity has been reported in this area (IGN, 2018). Moreover, in this region, two major historical earthquakes have occurred: the 1829 Torrevieja Earthquake (IMSK = IX-X;  $M_s = 6.3-6.9$ ), which caused nearly 400 casualties (Muñoz & Udías, 1991), and the 1919 Jacarilla-Torremendo earthquake ( $m_b = 5.1$  and  $5.2$ ). Furthermore, several examples of Quaternary deformation have been reported, including deformed alluvial fans and gullies (Goy & Zazo, 1989), uplifted marine terraces (Bousquet, 1979; Goy et al., 1993), mountain fronts (Silva et al., 2003), seismites (Alfaro et al., 1999), and tilted Pleistocene deposits (Dinarès-Turell et al., 1995). In addition, the study area is located in the EBSZ, which is a major tectonic structure with regional significance. Many geological (Ferrater et al., 2017; Martínez-Díaz et al., 2012; Gràcia et al., 2006; Moreno et al., 2015, 2016, among many others) and geodetic (Echeverría et al., 2013, 2015) studies have shown that the EBSZ is an active structure.

We consider that all of the abovementioned evidence allows us to rule out the hypothesis of zero residual velocity for the Bajo Segura Basin. Likewise, the slip rates reported for the western and central sectors of the EBSZ range from  $1.5 \pm 0.3$  to  $0.8 \pm 0.4$  mm/year (Ferrater et al., 2017; Echeverría et al., 2013, 2015; Martínez-Díaz et al., 2012, Gràcia et al., 2006; Moreno et al., 2015, 2016, among many others). Consequently, we postulate that the residual velocities obtained in the eastern EBSZ (our study area) should be similar to those reported in other sectors; that is, here, we discard the near-zero hypothesis.

## 6. Conclusions

The data presented here are the very first GPS observations obtained from the onshore termination of the EBSZ. This is a major tectonic structure with regional significance, as it extends from North Africa to southern Europe across the Trans-Alboran Betic Shear Zone. This major structure controls the present deformation in the eastern part of the Western Mediterranean region. The main issue with our data is the low signal-to-noise ratios of the residual velocities. These uncertainties are the consequence of the relatively slow (submillimetric) strain rate in this region. However, we consider our data to be sufficiently robust, as they are in good accordance with geological observations obtained at regional and local scales as well as with the geodetic data and models published in the literature.

Our basin-scale GPS study shows how detailed GPS analyses can contribute to a more precise understanding of the distribution of deformation in diffuse plate boundaries, such as the western Nubia-Eurasia region, by establishing its close relationship with active faults. The NE end of the EBSZ accommodates part of the shortening between Nubia and Eurasia ( $0.6 \pm 0.2$  mm/year), but we postulate that a significant part of this shortening must be distributed outside of this tectonic corridor, namely, to the north (External Betics) and to the south (the Cartagena Basin and its offshore neighboring area). We propose that the thin and rigid crust of the Algero-Balearic Basin acts as an indenter. This indenter transfers the Nubia-Eurasia convergence to the Eastern Betics.

The examination of our GPS data indicates that the plate convergence at the NE end of the EBSZ is partitioned. Two components can be distinguished in this sector of the EBSZ: a NNW-SSE shortening component and a N70E left-lateral component. This finding is consistent with local geology and the kinematics of the main active faults recognized in this area, that is, the CF and BSFZ. The blind reverse BSFZ accommodates  $0.2$  to  $0.7 \pm 0.2$  mm/year of shortening, while the fault slip rate of the left-lateral CF is  $0.8 \pm 0.2$  mm/year. These results are consistent with the geodynamic context of the EBSZ, which is characterized by transpression in the Eastern Betics.

## Acknowledgments

We acknowledge the comments of the two anonymous reviewers and the Associate Editor Glen S. Mattioli, which significantly improved the quality of this paper. This research was funded by the Spanish Ministry of Economy and Competitiveness (research project CGL2011-30153-C02-02), University of Alicante (research project VIGROB053), University of Jaén (PATUJA 2019/2020, CEACTierra), and RNM282 Research Group of Junta de Andalucía. We thank all observers who collected the data in survey-mode GPS measurements. All the data used are listed in the references or archived in the University of Alicante repository (<http://hdl.handle.net/10045/77387>).

## References

- Alfaro, P., Andreu, J. M., Bartolomé, R., Borque, M. J., Estévez, A., García-Mayordomo, J., et al. (2012). The Bajo Segura Fault Zone: Active blind thrusting in the Eastern Betic Cordillera (SE Spain). *Journal of Iberian Geology*, *38*(1), 271–284.
- Alfaro, P., Andreu, J. M., Delgado, J., Estévez, A., Soria, J. M., & Teixido, T. (2002). Quaternary deformation of the Bajo Segura blind fault (eastern Betic Cordillera, Spain) revealed by high-resolution reflection profiling. *Geological Magazine*, *139*(3), 331–341. <https://doi.org/10.1017/S0016756802006568>
- Alfaro, P., Delgado, J., Estévez, A., Soria, J. M., & Yébenes, A. (2002). Onshore and offshore compressional tectonics in the eastern Betic Cordillera (SE Spain). *Marine Geology*, *186*(3–4), 337–349. [https://doi.org/10.1016/S0025-3227\(02\)00336-5](https://doi.org/10.1016/S0025-3227(02)00336-5)
- Alfaro, P., Estévez, A., Moretti, M., & Soria, J. M. (1999). Structures sédimentaires de déformation interprétées comme séismites dans le Quaternaire du bassin du Bas Segura (Cordillère Bétique orientale). *Comptes Rendues Academie Sciences. Paris (II)*, *328*(1), 17–22.
- Altamimi, Z., Métivier, L., & Collilieux, X. (2012). ITRF2008 plate motion model. *Journal of Geophysical Research*, *117*, B07402. <https://doi.org/10.1029/2011JB008930>
- Argus, D. F., Gordon, R. G., & DeMets, C. (2011). Geologically current motion of 56 plates relative to the no-net-rotation reference frame. *Geochemistry, Geophysics, Geosystems*, *12*, Q11001. <https://doi.org/10.1029/2011GC003751>
- Baratin, L. M., Mazzotti, S., Vernant, J. C. P., Tahayt, A., & Mourabit, T. (2016). Incipient mantle delamination, active tectonics and crustal thickening in Northern Morocco: Insights from gravity data and numerical modeling. *Earth and Planetary Science Letters*, *454*, 113–120. <https://doi.org/10.1016/j.epsl.2016.08.041>
- Batló, J., Martínez-Solares, J. M., Macià, R., Stich, D., Morales, J., & Garrido, L. (2015). The autumn 1919 Torremendo (Jacarilla) earthquake series (SE Spain). *Annals of Geophysics*, *58*(3), S0324. <https://doi.org/10.4401/ag-6686S0324>
- Beavan, J., Wallace, L. M., Palmer, N., Denys, P., Ellis, S., Fournier, N., et al. (2016). New Zealand GPS velocity field: 1995–2013. *New Zealand Journal of Geology and Geophysics*, *59*(1), 5–14. <https://doi.org/10.1080/00288306.2015.1112817>
- Bertiger, W., Desai, S., Haines, B., Harvey, N., Moore, A. W., Owen, S., & Weiss, J. P. (2010). Single receiver phase ambiguity resolution with GPS data. *Journal of Geodesy*, *84*(5), 327–337. <https://doi.org/10.1007/s00190-010-0371-9>
- Bilitza, D. (2001). International reference ionosphere 2000. *Radio Science*, *36*(2), 261–275. <https://doi.org/10.1029/2000RS002432>
- Booth-Rea, G., Ranero, C. R., Martínez-Martínez, J. M., & Grevemeyer, I. (2007). Crustal types and Tertiary tectonic evolution of the Alborán sea, western Mediterranean. *Geochemistry, Geophysics, Geosystems*, *8*, Q10005. <https://doi.org/10.1029/2007GC001639>
- Bousquet, J. C. (1979). Quaternary strike-slip faults in Southeastern Spain. *Tectonophysics*, *52*(1–4), 277–286. [https://doi.org/10.1016/0040-1951\(79\)90232-4](https://doi.org/10.1016/0040-1951(79)90232-4)
- Bufo, E., Sanz de Galdeano, C., & Udías, A. (1995). Seismotectonics of the Ibero-Maghrebian región. *Tectonophysics*, *248*, 247–261. [https://doi.org/10.1016/0040-1951\(94\)00276-F](https://doi.org/10.1016/0040-1951(94)00276-F)
- Comas, M. C., Platt, J. P., Soto, J., & Watts, A. B. (1999). The origin and tectonic history of the Alborán Basin: Insights from Leg 161 results. In R. Zahn, M. C. Comas, & A. Klaus (Eds.), *Proceedings of the Ocean Drilling Program, Scientific Results* (Vol. 161, pp. 555–579). College Station, USA: Ocean Drilling Program. <https://doi.org/10.2973/odp.proc.sr.161.1999>
- De Guidi, G., Lanzafame, G., Palano, M., Puglisi, G., Scaltrito, A., & Scarfi, L. (2013). Multidisciplinary study of the Tindari Fault (Sicily, Italy) separating ongoing contractional and extensional compartments along the active Africa-Eurasia convergent boundary. *Tectonophysics*, *588*, 1–17. <https://doi.org/10.1016/j.tecto.2012.11.021>
- De Larouzière, F., Bolze, J. J., De Larouzière, F. D., Montenat, C., & Ott d'Estevou, P. (1988). The Betic segment of the lithospheric trans-Alboran shear zone during the late Miocene. *Tectonophysics*, *152*(1–2), 41–52. [https://doi.org/10.1016/0040-1951\(88\)90028-5](https://doi.org/10.1016/0040-1951(88)90028-5)
- DeMets, C., Gordon, R. G., & Argus, D. F. (2010). Geologically current plate motions. *Geophysical Journal International*, *181*(1), 1–80. <https://doi.org/10.1111/j.1365-246X.2009.04491.x>
- Desai, S. D., Bertiger, W., Haines, B., Harvey, N., Selle, C., Sibthorpe, A., & Weiss, J. P. (2011). Results from the reanalysis of global GPS data in the IGS08 reference frame. AGU Fall Meeting Abstracts, 1, 0904.
- Dinarès-Turell, J., Alfaro, P., & Soria, J. (1995). A deformed Pliocene–Quaternary alluvial and red paleosol succession in the eastern Betics: Paleomagnetic, rock-magnetic and sedimentological pilot study. *Studia Geophysica et Geodaetica*, *39*(4), 405–419. <https://doi.org/10.1007/BF02295894>
- Echeverría, A., Khazaradze, G., Asensio, E., Gárate, J., Martín-Dávila, J., & Suriñach, E. (2013). Crustal deformation in eastern Betics from CuaTeNeo GPS network. *Tectonophysics*, *608*, 600–612. <https://doi.org/10.1016/j.tecto.2013.08.020>
- Echeverría, A., Khazaradze, G., Asensio, E., & Masana, E. (2015). Geodetic evidence for continuing tectonic activity of the Carboneras Fault (SE Spain). *Tectonophysics*, *663*, 302–309. <https://doi.org/10.1016/j.tecto.2015.08.009>
- Fadil, A., Vernant, P., McClusky, S., Reilinger, R., Gomez, F., Ben Sari, D., et al. (2006). Active tectonics of the western Mediterranean: Geodetic evidence for rollback of a delaminated subcontinental lithospheric slab beneath the Rif Mountains, Morocco. *Geology*, *34*(7), 529–532. <https://doi.org/10.1130/G22291.1>
- Fernandes, R. M. S., Miranda, J. M., Meijninger, B. M. L., Bos, M. S., Noomen, R., Bastos, L., et al. (2007). Surface velocity field of the Ibero-Maghrebian segment of the Eurasia-Nubia plate boundary. *Geophysical Journal International*, *169*(1), 315–324. <https://doi.org/10.1111/j.1365-246X.2006.03252.x>
- Ferranti, L., Palano, M., Cannavo, F., Mazzella, M. E., Oldow, J., Gueguen, E., et al. (2014). Rates of geodetic deformation across active faults in southern Italy. *Tectonophysics*, *621*, 101–122. <https://doi.org/10.1016/j.tecto.2014.02.007>
- Ferrater, M., Ortuño, M., Masana, E., Martínez-Díaz, J. J., Pallás, R., & Perea, H. (2017). Lateral slip rate of Alhama de Murcia fault (SE Iberian Peninsula) based on a morphotectonic analysis: Comparison with paleoseismological data. *Quaternary International*, *451*, 87–100. <http://doi.org/10.1016/j.quaint.2017.02.018>
- Galindo Zaldívar, J., Gil, A. J., Borque, M. J., González-Lodeiro, F., Jabaloy, A., Marín-Lechado, C., et al. (2003). Active faulting in the internal zones of the central Betic Cordilleras (SE, Spain). *Journal of Geodynamics*, *36*(1–2), 239–250. [https://doi.org/10.1016/S0264-3707\(03\)00049-8](https://doi.org/10.1016/S0264-3707(03)00049-8)
- Galindo-Zaldívar, J., Gil, A. J., Sanz de Galdeano, C., Lacy, M. C., García-Armenteros, J. A., Ruano, P., et al. (2015). Active shallow extensión in central and Eastern Betic Cordillera from CGPS data. *Tectonophysics*, *663*, 290–301. <https://doi.org/10.1016/j.tecto.2015.08.035>
- Galindo-Zaldívar, J., González-Lodeiro, F., & Jabaloy, A. (1993). Stress and paleostress in the Betic-Rif Cordilleras (Miocene to present-day). *Tectonophysics*, *227*(1–4), 105–126. [https://doi.org/10.1016/0040-1951\(93\)90090-7](https://doi.org/10.1016/0040-1951(93)90090-7)
- García Mayordomo, J. (2005). *Caracterización y análisis de la peligrosidad sísmica en el sureste de España*. PhD Doctoral Thesis. Madrid, Spain, 373: Universidad Complutense de Madrid, Madrid.

- García-Mayordomo, J., & Martínez-Díaz, J. J. (2006). Caracterización sísmica del anticlinorio del Bajo Segura (Alicante): Fallas del Bajo Segura, Torrevieja y San Miguel de Salinas. *Geogaceta*, *40*, 19–22.
- Gauyau, F., Bayer, R., Bousquet, J. C., Lachaud, J. C., Lesquer, A., & Montenat, C. (1977). Le prolongement de l'accident d'Alhama de Murcia et Alicante (Espagne méridionale). *Bulletin de la Société Géologique de France*, *XXII*, *3*, 501–509.
- Gil, A. J., Rodríguez-Caderot, G., de Lacy, M. C., Ruiz, A. M., Sanz de Galdeano, C., & Alfaro, P. (2002). Establishment of a non-permanent GPS network to monitor the recent NE-SW deformation in the Granada basin (Betic Cordillera, Southern Spain). *Studia Geophysica et Geodaetica*, *46*(3), 395–410. <https://doi.org/10.1023/A:1019530716324>
- Giménez, J., Borque, M. J., Gil, A., Alfaro, P., Estévez, A., & Suriñach, E. (2009). Comparison of long-term and short-term uplift rates along an active blind reverse fault zone (Bajo Segura, SE Spain). *Studia Geophysica et Geodaetica*, *53*, 81–98. <https://doi.org/10.1007/s11200-009-0005>
- Giner, J. J., Molina, S., & Jáuregui, P. J. (2003). Sismicidad en la Comunidad Valenciana (C.V.). *Física de la Tierra*, *15*, 163–187.
- Goy, J. L., & Zazo, C. (1989). The role of neotectonics in the morphologic distribution of the Quaternary marine and continental deposits of the Elche Basin, southeast Spain. *Tectonophysics*, *163*(3-4), 219–225. [https://doi.org/10.1016/0040-1951\(89\)90259-X](https://doi.org/10.1016/0040-1951(89)90259-X)
- Goy, J. L., Zazo, C., Bardaji, T., Somoza, L., Causse, C., & Hillaire-Marcel, C. (1993). Elements d'une chronostratigraphie du Tyrrhénien des régions d'Alicante-Murcia, Sud-Est de l'Espagne. *Geodinamica Acta*, *6*(2), 103–119.
- Gràcia, E., Pallàs, R., Soto, J. I., Comas, M., Moreno, X., Masana, E., et al. (2006). Active faulting offshore SE Spain (Alboran Sea): Implications for Earthquake hazard assessment in the south Iberian margin. *Earth and Planetary Science Letters*, *241*, 734–749. <https://doi.org/10.1016/j.epsl.2005.11.009>
- Gutscher, M. A., Malod, J., Rehault, J. P., Contrucci, I., Klingelhoefer, F., Mendes-Victor, L., & Spakman, W. (2002). Evidence for active subduction beneath Gibraltar. *Geology*, *30*(12), 1071–1074. [https://doi.org/10.1130/0091-7613\(2002\)030<1071:EFASBG>2.0.CO;2](https://doi.org/10.1130/0091-7613(2002)030<1071:EFASBG>2.0.CO;2)
- I.G.M.E. (2015). QAFI: Quaternary-active faults database of Iberia. Accessed 15, December, 2017
- IGN (2015). Spanish seismic hazard map. IGN-Instituto Geográfico Nacional. Mapa de peligrosidad sísmica de España <http://www.ign.es/web/mapas-sismicidad>. Accessed 4, June, 2018
- IGN (2018). Spanish seismic catalogue. IGN-Instituto Geográfico Nacional. Catálogo Sísmico Nacional <http://www.ign.es>. Accessed 4, June, 2018
- Koullali, A., Ouazar, D., Tahayt, A., King, R. W., Vernant, P., Reilinger, R. E., et al. (2011). New GPS constraints on active deformation along the Africa–Iberia plate boundary. *Earth and Planetary Science Letters*, *308*(1-2), 211–217. <https://doi.org/10.1016/j.epsl.2011.05.048>
- Lyard, F., Lefevre, F., Letellier, T., & Francis, O. (2006). Modelling the global ocean tides: modern insights from FES2004. *Ocean Dynamics*, *56*(5-6), 394–415. <https://doi.org/10.1007/s10236-006-0086-x>
- Maillard, A., & Mauffret, A. (2013). Structure and present-day compression in the offshore area between Alicante and Ibiza Island (Eastern Iberian Margin). *Tectonophysics*, *591*, 116–130. <https://doi.org/10.1016/j.tecto.2011.07.007>
- Marín-Lechado, C., Galindo-Zaldívar, J., Gil, A. J., Borque, M. J., De Lacy, C., Pedrera, A., et al. (2010). Levelling profiles and GPS network to monitor the active folding and faulting deformation in the Campo de Dalías (Betic Cordillera, Southeastern Spain). *Sensors*, *10*(4), 3504–3518. <https://doi.org/10.3390/s100403504>
- Martín-Algarra, A., & Vera, J. A. (2004). La Cordillera Bética y las Baleares en el contexto del Mediterráneo Occidental. In J. A. Vera (Ed.), *Geología de España* (pp. 352–354). Madrid: Sociedad Geológica de España. Instituto Geológico y Minero de España.
- Martín-Banda, R., García-Mayordomo, J., Insua-Arevalo, J. M., Salazar, A. E., Rodríguez-Escudero, E., Alvarez-Gomez, J. A., et al. (2016). New insights on the seismogenic potential of the Eastern Betic Shear Zone (SE Iberia): Quaternary activity and paleoseismicity of the SW segment of the Carrascoy Fault Zone. *Tectonics*, *35*, 55–75. <https://doi.org/10.1002/2015TC003997>
- Martínez-Díaz, J. J., Béjar-Pizarro, M., Álvarez-Gómez, J. A., Lis Mancilla, F., Stich, D., Herrera, G., & Morales, J. (2012). Tectonic and seismic implications of an intersegment rupture: The damaging May 11th 2011  $M_w$  5.2 Lorca, Spain, earthquake. *Tectonophysics*, *546*–547, 28–37. <https://doi.org/10.1016/j.tecto.2012.04.010>
- Martín-Rojas, I., Alfaro, P., & Estévez, A. (2014). Evolución tectónica del borde norte de la Cuenca del Bajo Segura. Implicaciones en la evolución de la Falla de Crevillente (sector Abanilla-Alicante). *Cuaternario y Geomorfología*, *28*(3–4), 85–94.
- Martín-Rojas, I., Alfaro, P., & Estévez, A. (2015). 3D geometry of growth strata in a fault-propagation fold. Insights into space-time evolution of the Crevillente Fault (Abanilla-Alicante sector), Betic Cordillera, Spain. *International Journal of Earth Sciences*, *104*, 1387–1404. <https://doi.org/10.1007/s00531-015-1143-9>
- Masana, E., Martínez-Díaz, J. J., Hernández-Enrile, J. L., & Santanach, P. (2004). The Alhama de Murcia fault (SE Spain), a seismogenic fault in a diffuse plate boundary: seismotectonic implications for the Ibero–Magrebian region. *Journal of Geophysical Research*, *109*, B01301. <https://doi.org/10.1029/2002JB002359>
- McClusky, S., Reilinger, R., Mahmoud, S., Ben Sari, D., & Tealeb, A. (2003). GPS constraints on Africa (Nubia) and Arabia plate motions. *Geophysics Journal International*, *155*(1), 126–138. <https://doi.org/10.1046/j.1365-246X.2003.02023.x>
- Montenat, C. (1977). Les bassins néogènes et quaternaires du Levant d'Alicante à Murcie (Cordillères bétiques orientales, Espagne). Stratigraphie, paléontologie et evolution dynamique. Documents des laboratoires de géologie de la Faculté des Sciences de Lyon, *69*, 345 p.
- Montenat, C., Ott d'Estevou, P., & Coppier, G. (1990). Les bassins néogènes entre Alicante et Cartagena (Espagne). *Doc. et Trav. I.G.A.L.*, *12*-13, 313-368.
- Moreno, X., Gràcia, E., Bartolomé, R., Martínez-Lorient, S., Perea, H., de la Peña, L. G., et al. (2016). Seismostratigraphy and tectonic architecture of the Carboneras Fault offshore based on multiscale seismic imaging: Implications for the Neogene evolution of the NE Alboran Sea. *Tectonophysics*, *689*, 115–132. <https://doi.org/10.1016/j.tecto.2016.02.018>
- Moreno, X., Masana, E., Pallàs, R., Gràcia, E., Rodés, Á., & Bordonau, J. (2015). Quaternary tectonic activity of the Carboneras Fault in the La Serrata range (SE Iberia): Geomorphological and chronological constraints. *Tectonophysics*, *663*, 78–94. <https://doi.org/10.1016/j.tecto.2015.08.016>
- Mueller, M. D., Geiger, A., Kahle, H. G., Veisb, G., Billiris, H., Paradissis, D., & Felekis, S. (2013). Velocity and deformation fields in the North Aegean domain, Greece, and implications for fault kinematics, derived from GPS data 1993-2009. *Tectonophysics*, *597*, 34–49.
- Muñoz, D., & Udías, A. (1991). Three large historical earthquakes in Southern Spain. In J. Mézcua & A. Udías (Eds.), *Seismicity, seismotectonics and seismic risk of the Ibero-Maghrebian region* (Vol. 8, pp. 175–182). Madrid: Instituto Geográfico Nacional Madrid.
- Noçquet, J. M. (2012). Present-day kinematics of the Mediterranean: A comprehensive overview of GPS results. *Tectonophysics*, *579*, 220–242. <https://doi.org/10.1016/j.tecto.2012.03.037>
- Oláiz, A. J., Muñoz-Martín, A., De Vicente, G., Vegas, R., & Cloetingh, S. (2009). European continuous active tectonic strain–stress map. *Tectonophysics*, *474*(1–2), 33–40. <https://doi.org/10.1016/j.tecto.2008.06.023>

- Palano, M., González, P. J., & Fernández, J. (2013). Strain and stress fields along the Gibraltar Orogenic Arc: Constraints on active geodynamics. *Gondwana Research*, 23(3), 1071–1088. <https://doi.org/10.1016/j.gr.2012.05.021>
- Palano, M., González, P. J., & Fernández, J. (2015). The diffuse plate boundary of Nubia and Iberia in the Western Mediterranean: Crustal deformation evidence for viscous coupling and fragmented lithosphere. *Earth and Planetary Science Letters*, 430, 439–447. <https://doi.org/10.1016/j.epsl.2015.08.040>
- Perea, H., Gràcia, E., Alfaro, P., Bartolomé, R., Lo Iacono, C., Moreno, X., Masana, E., & EVENT-SHELF Team (2012). Structure and potential seismogenic sources of the offshore Bajo Segura basin (SE Iberian Peninsula, Mediterranean Sea). *Natural Hazards and Earth System Sciences*, 12(10), 3151–3168. <https://doi.org/10.5194/nhess-12-3151-2012>
- Pérez-Peña, J. V., Azor, A., Azañón, J. M., & Keller, E. A. (2010). Active tectonics in the Sierra Nevada (Betic Cordillera, SE Spain): Insights from geomorphic indexes and drainage pattern analysis. *Geomorphology*, 119(1-2), 74–87. <https://doi.org/10.1016/j.geomorph.2010.02.020>
- Pérouse, E., Vernant, P., Chéry, J., Reilinger, R., & McClusky, S. (2010). Active surface deformation and sub-lithospheric processes in the western Mediterranean constrained by numerical models. *Geology*, 38(9), 823–826. <https://doi.org/10.1130/G30963.1>
- Petit, C., Le Pourhiet, L., Scalabrino, B., Corsini, M., Bonnín, M., & Romagny, A. (2015). Crustal structure and gravity anomalies beneath the Rif, northern Morocco: implications for the current tectonics of the Alboran region. *Geophysical Journal International*, 202(1), 640–652. <https://doi.org/10.1093/gji/ggv169>
- Ruiz, A. M., Ferhat, G., Alfaro, P., Sanz de Galdeano, C., de Lacy, C., Rodríguez-Caderot, G., & Gil, A. J. (2003). Geodetic measurements of crustal deformation on NW-SE faults of the Betic Cordillera, southern Spain. *Journal of Geodynamics*, 35(3), 259–272. [https://doi.org/10.1016/S0264-3707\(02\)00134-5](https://doi.org/10.1016/S0264-3707(02)00134-5)
- Sánchez-Alzola, A., Borque, M. J., Martín-Rojas, I., García-Tortosa, F. J., Alfaro, P., Estévez, A., & Gil, A. J. (2014). Tasas de deformación GPS en la Cuenca del Bajo Segura (Cordillera Bético-Oriental). *Geogaceta*, 56, 3–6.
- Sanz de Galdeano, C. (1983). Los accidentes y fracturas principales de las cordilleras Béticas. *Estudios Geológicos*, 39, 157–165.
- Sanz de Galdeano, C., & Buforn, E. (2005). From strike-slip to reverse reactivation: The Crevillente Fault system and seismicity in the Bullas-Mula area (Betic Cordillera, SE Spain). *Geologica Acta*, 3, 241–250.
- Sella, G. F., Dixon, T. H., & Mao, A. (2002). REVEL: A model for recent plate velocities from space geodesy. *Journal of Geophysical Research*, 107(B4), ETG 11-1–ETG 11-30. <https://doi.org/10.1029/2000JB000033>
- Serpelloni, E., Vannucci, G., Pondrelli, S., Argnanì, A., Casula, G., Anzidei, M., et al. (2007). Kinematics of the western Africa-Eurasia plate boundary from focal mechanisms and GPS data. *Geophysical Journal International*, 169(3), 1180–1200. <https://doi.org/10.1111/j.1365-246X.2007.03367>
- Shen, Z.-K., King, R. W., Agnew, D. C., Wang, M., Herring, T. A., Dong, D., & Fang, P. (2011). A unified analysis of crustal motion in Southern California, 1970–2004: The SCEC crustal motion map. *Journal of Geophysical Research*, 116, B11402. <https://doi.org/10.1029/2011JB008549>
- Silva, P. G., Goy, J. L., Somoza, L., Zazo, C., & Bardaji, T. (1993). Landscape response to strike-slip faulting linked to collisional setting: Quaternary tectonics and basin formation in the Eastern Betics, southeastern Spain. *Tectonophysics*, 224(4), 289–303. [https://doi.org/10.1016/0040-1951\(93\)90034-H](https://doi.org/10.1016/0040-1951(93)90034-H)
- Silva, P. G., Goy, J. L., Zazo, C., & Bardaji, T. (2003). Fault-generated mountain fronts in southeast Spain: Geomorphologic assessment of tectonic and seismic activity. *Geomorphology*, 50(1-3), 203–225. [https://doi.org/10.1016/S0169-555X\(02\)00215-5](https://doi.org/10.1016/S0169-555X(02)00215-5)
- Soria, J., Alfaro, P., Fernández, J., & Viseras, C. (2001). Quantitative subsidence-uplift analysis on the Bajo Segura Basin (eastern Betic Cordillera, Spain): Tectonic control on the stratigraphic architecture. *Sedimentary Geology*, 140(3-4), 271–289. [https://doi.org/10.1016/S0037-0738\(00\)00189-5](https://doi.org/10.1016/S0037-0738(00)00189-5)
- Spakman, W., Chertova, M. V., van den Berg, A., & van Hinsbergen, D. J. J. (2018). Puzzling features of western Mediterranean tectonics explained by slab dragging. *Nature Geoscience*, 11(3), 211–216. <https://doi.org/10.1038/s41561-018-0066-z>
- Stich, D., Serpelloni, E., de Lis Mancilla, F., & Morales, J. (2006). Kinematics of the Iberia-Maghreb plate contact from seismic moment tensors and GPS observations. *Tectonophysics*, 426(3-4), 295–317. <https://doi.org/10.1016/j.tecto.2006.08.004>
- Stirling, M., Rhoades, D., & Berryman, K. (2002). Comparison of earthquake scaling relations derived from data of the instrumental and preinstrumental era. *Bulletin of the Seismological Society of America*, 92(2), 812–830. <https://doi.org/10.1785/0120000221>
- Taboada, A., Bousquet, J. C., & Philip, H. (1993). Co-seismic elastic models of folds above blind thrusts in the Betic Cordilleras (Spain) and evaluation of seismic hazard. *Tectonophysics*, 220, 223–241. [https://doi.org/10.1016/0040-1951\(93\)90233-A](https://doi.org/10.1016/0040-1951(93)90233-A)
- Teza, G., Pesci, A., & Galgaro, A. (2008). Grid\_strain and grid\_strain3: Software packages for strain field computation in 2D and 3D environments. *Computers & Geosciences*, 34(9), 1142–1153. <https://doi.org/10.1016/j.cageo.2007.07.006>
- Vernant, P., Fadil, A., Mourabit, T., Ouazar, D., Koulali, A., Martin-Davila, J., et al. (2010). Geodetic constraints on active tectonics of the Western Mediterranean: Implications for the kinematics and dynamics of the Nubia-Eurasia plate boundary zone. *Journal of Geodynamics*, 49(3–4), 123–129. <http://doi.org/10.1016/j.jog.2009.10.007>
- Zumberge, J. F., Heflin, M. B., Jefferson, D. C., Watkins, M. M., & Webb, F. H. (1997). Precise point positioning for the efficient and robust analysis of GPS data from large networks. *Journal of Geophysical Research*, 102(B3), 5005–5017. <https://doi.org/10.1029/96JB03860>